



HAL
open science

Magnetic properties of perpendicularly magnetized [Au/Co/Pd] n thin films and nanostructures with Dzyaloshinskii-Moriya interaction

Chloé Bouard, Patrick Warin, Alain Marty, Laurent Vila, van Tuong Pham,
Jean-Philippe Attané

► To cite this version:

Chloé Bouard, Patrick Warin, Alain Marty, Laurent Vila, van Tuong Pham, et al.. Magnetic properties of perpendicularly magnetized [Au/Co/Pd] n thin films and nanostructures with Dzyaloshinskii-Moriya interaction. AIP Advances, 2018, 8 (9), pp.095315. 10.1063/1.5036616 . cea-01962480

HAL Id: cea-01962480

<https://cea.hal.science/cea-01962480>

Submitted on 20 Dec 2018

HAL is a multi-disciplinary open access archive for the deposit and dissemination of scientific research documents, whether they are published or not. The documents may come from teaching and research institutions in France or abroad, or from public or private research centers.

L'archive ouverte pluridisciplinaire **HAL**, est destinée au dépôt et à la diffusion de documents scientifiques de niveau recherche, publiés ou non, émanant des établissements d'enseignement et de recherche français ou étrangers, des laboratoires publics ou privés.

Magnetic properties of perpendicularly magnetized [Au/Co/Pd]_n thin films and nanostructures with Dzyaloshinskii-Moriya interaction

Chloé Bouard, Patrick Warin, Alain Marty, Laurent Vila, Van Tuong Pham, and Jean-Philippe Attané^a
Univ. Grenoble Alpes, CEA, CNRS, Grenoble INP, INAC, SPINTEC, F-38000 Grenoble, France

(Received 17 April 2018; accepted 23 August 2018; published online 18 September 2018)

Magnetic force microscopy imaging enable to extract the main magnetic parameters (saturation magnetization, anisotropy, domain size, exchange constant). The magnetoresistance and the extraordinary Hall effect of the material have been characterized using nanostructures patterned on the multilayer. Both the magnetization reversal mode and the magnetotransport properties are found to depend strongly on the nanowire width. The relatively low coercive field, the high anisotropy, and the possibility to control domain wall motion in sub-100 nm wires make this system an interesting alternative to Pt-based multilayers for spin-transfer torques experiments. © 2018 Author(s). All article content, except where otherwise noted, is licensed under a Creative Commons Attribution (CC BY) license (<http://creativecommons.org/licenses/by/4.0/>). <https://doi.org/10.1063/1.5036616>

Materials with perpendicular magnetic anisotropy and high Dzyaloshinskii-Moriya interaction (DMI) have recently attracted a large interest for spin-transfer torque applications based on domain walls (DW) and skyrmions. Indeed, the possibility to repel the Walker breakdown^{1,2} and to stabilize Néel walls^{3,4} or skyrmions in films⁵ or nanostructures⁶⁻⁸ could be the basis of new memory and logic devices.^{9,10}

Most experiments have been realized in bilayers or trilayers, including a layer of heavy metal and an ultrathin Co⁸ or Fe layer.¹¹ In the case of single bilayers or trilayers, the magnetic texture has been found to be stable only at very low temperature,^{12,13} and magnetic fields are required to stabilize a single metastable skyrmion.¹⁴

Another route is the development of thick [metal 1/ferromagnet/metal 2]_n multilayers, or of [metal/ferromagnet/oxide]_n stacks, such as [Ir/Co/Pt]₁₀,¹⁵ [Pt/Co/Ta]₁₅ and [Pt/CoFeB/MgO]₁₅.¹⁶ In such materials, the interface effects could provide both the DMI and the perpendicular anisotropy, while conserving the lack of inversion symmetry at the vicinity of the ferromagnetic layer. It becomes possible to reach thicknesses large enough to facilitate skyrmions or DWs observation, to enhance their thermal stability,^{15,16} and to enable the measurement of the topological Hall effect.^{17,20} The use of multilayers could help tuning precisely the magnetic parameters such as the DMI, the anisotropy and the saturation magnetization.¹⁸⁻²¹ More importantly, it would allow developing stacks in which most of the current used to induce DW or skyrmion motion would go through the magnetic part.²⁰

In this context, *ab initio* calculations²² have recently predicted that [Au/Co/Pd]_n multilayers are an interesting system to perform spin-transfer experiments, thanks to the opposite DMI signs of the Co/Pd and Co/Au interfaces.

In this article, we study the magnetization reversal and magnetotransport properties of [Au (10 Å)/Co (6.6 Å)/Pd (10 Å)]₁₀ thin films and nanostructures. The magnetoresistance (MR)

^aJean-philippe.attane@cea.fr

and the extraordinary Hall effect (EHE) of the material have been measured using nanostructures patterned on the multilayer. Both the magnetization reversal, which occurs by DW propagation, and the magnetotransport properties, are found to depend strongly on the nanowire width.

[Au (10 Å)/Co (6.6 Å)/Pd (10 Å)]₁₀ multilayers have been grown by DC magnetron sputtering on a silicon oxide substrate, with a Ti (5 Å)/Au (50 Å) buffer layer, and a Au (30 Å) capping layer to prevent oxidation. The magnetic properties of the sample have been measured using a SQUID magnetometer. The hysteresis loops for an in-plane and an out-of-plane applied field are shown in Fig. 1a. The multilayer is found to possess an out-of-plane magnetization, with a saturation magnetization of 1400 ± 100 kA/m and a large perpendicular anisotropy $K_{eff} = 150 \pm 10$ kJ/m³ (estimated from the area between in-plane and perpendicular magnetization curves), comparable to that of Co/Pt²³ or Co/Ni²⁴ multilayers. The saturation magnetization has been calculated considering the ten 6.6 Å-thick layers of cobalt. The hysteresis loop for out-of-plane fields exhibit a remanence of around 30 %, and a relatively low coercive field of 14.5 ± 0.2 mT.

Fig. 1b shows the magnetic configuration of an as-grown thin film, observed by magnetic force microscopy (MFM). The structure of interlaced up and down domains is characteristic of layers with perpendicular magnetization, with a mean domain width of around 135 ± 5 nm (evaluated from the Fourier transform of the MFM images). Note that the mean domain width is also found to be around 135 nm after demagnetization, so that we can suppose that the observed domain width is close to the equilibrium domain width.

The equilibrium width results from the competition between the DW energy and the demagnetizing field energy. Using the analytical model proposed by Kaplan and Gehring,²⁵ and modified by Gehanno *et al.*,²⁶ it is possible to extract the DW energy $\sigma_{DW} = 2.6 \pm 0.2$ mJ/m². The energy of a Bloch DW is $\sigma_{DW} = 4\sqrt{AK_{eff}}$, with A the exchange stiffness. Considering $A = 5 - 15$ pJ/m (values reported in literature for Co), we find $\sigma_{DW} = 3.5 - 6.0$ mJ/m², which is larger than the value calculated from the equilibrium width of magnetic domains. This could indicate the presence of the DMI, as the DMI is known to lower the DW energy by a value equal to πD ,²⁷ D being the DMI constant. The DMI constant value extracted from the DW energy would thus be of 0.7 ± 0.4 mJ/m², slightly smaller than the theoretical prediction of 1.25 mJ/m² obtained by adding the two Co/Pd and Co/Au contributions calculated ab-initio,²² and smaller than what can be obtained using Pt.¹⁵ Note however that this value

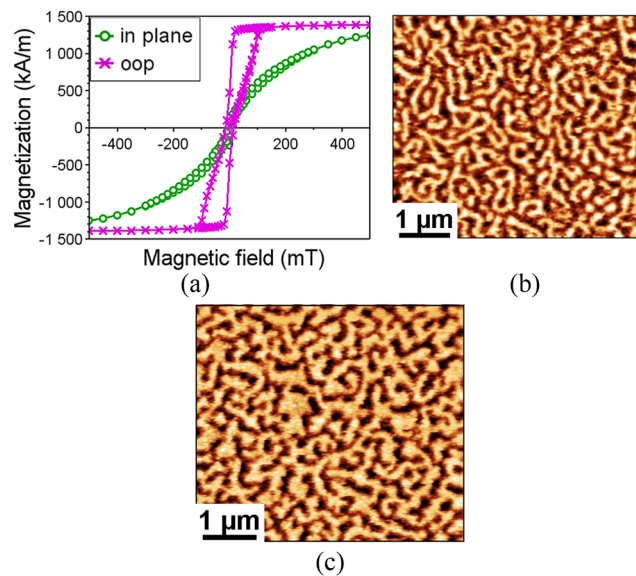


FIG. 1. a) In-plane and out-of-plane hysteresis loops at room temperature, measured using a SQUID magnetometer. $5 \times 5 \mu\text{m}^2$ MFM image of the magnetic domains b) in an as-grown sample and c) in the remanent state after magnetic saturation.

has to be taken cautiously. Further experiments could allow determining more precisely the strength of the DMI.^{28,29}

Fig. 1c shows the magnetic configuration observed by MFM in the remanent state, after saturation. The reversed domains appear in black. The DWs are less smooth than what was observed in the as-grown state: there is indeed a competition during the growth between the disorder (*i.e.*, the pinning of DWs on structural defects), which tends to roughen the DW, the domain wall energy, which tends to smooth it, and the demagnetizing field effects, which try to impose the equilibrium domain size.³⁰

The resulting domain width of the growth process remains close to the equilibrium (135 ± 5 nm), which means that the domain structure is mostly governed by demagnetizing field effects. The coercivity, which is due to DW pinning, is relatively small ($H_C = 14.5 \pm 0.2$ mT). It is comparable to that of typical $[\text{Co/Pt}]_n$ multilayers with perpendicular anisotropy,³¹ so that one can expect to observe current-induced DW motion at zero field.

The samples have been patterned into double Hall crosses separated, using e-beam lithography on a negative resist and ion milling (cf. Fig. 2a), with wire widths of 100, 200 and 500 nm. The wires are connected to large areas serving both as electrical contacts and domain nucleation pads. The devices have then been wire-bonded to perform magnetotransport measurements. The longitudinal and Hall resistances have been measured using a lock-in amplifier, working at 107 Hz, and with an applied current of 100 μA .

The temperature dependence of the longitudinal resistivity of the entire stack is given on Fig. 2b. The resistivity, which depends on the quality of the sample, is reasonably small ($\rho_{xx} = 24.3$ $\mu\Omega\cdot\text{cm}$ at 300 K, with a RRR $\rho_{xx}(300\text{ K})/\rho_{xx}(10\text{ K}) = 1.3$). The longitudinal MR and the EHE have been measured in thin films and in the double Hall crosses, the magnetic field being applied perpendicular to the specimen. The evolution of these magnetotransport properties as a function of the width of the wires is presented on Fig. 3.

The measurement of the EHE on the thin film is consistent with the SQUID measurements of Fig. 1a. The EHE measurements in the Hall crosses allow to extract the EHE angle of the whole stack. The EHE angle is found to be $\theta_{EH} = \rho_{EHE}/\rho_{xx} = 0.44$ % at room temperature and at 10K, close to $[\text{Pt/Co}]_n$ multilayers (1.3 % for similar thicknesses).³¹ Note that, since part of the current is shunted by the Au buffer layer, this value has to be considered as a lower bound of the EHE angle of the $[\text{Au/Co/Pd}]_{10}$ multilayer.

The MR curve presents at high fields a non-saturating linear decrease of the resistance, which can be attributed to the magnon magnetoresistance (MMR), *i.e.*, to the contribution of magnons to the resistivity.³² The value of $\frac{d\rho}{dB}$ at room temperature is 0.04 $\mu\Omega\cdot\text{cm}\cdot\text{T}^{-1}$ or 0.2 %/T for the whole stack, comparable to that of FePt³⁴ and NiFe,³³ so that the MMR could be used to detect DW motion.³⁴

The MR curves of Fig. 3b also present a hysteretic behavior at low fields, with an increase of resistance due to the MMR, with possible additional contributions from the anisotropic MR and the DW resistance.³⁵

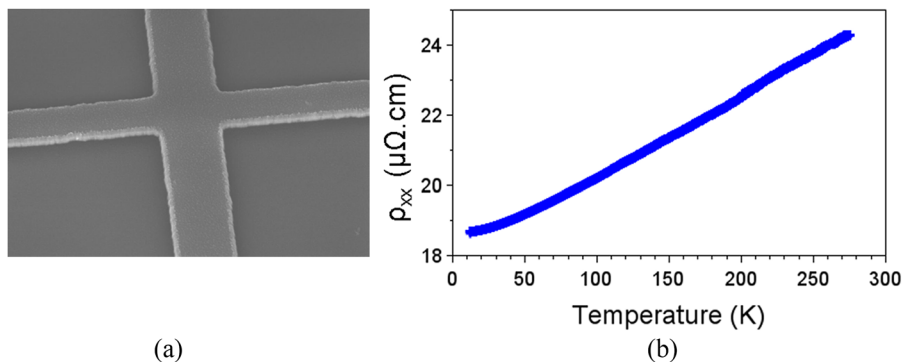


FIG. 2. a) Scanning electron microscopy image of a 500 nm wide cross (tilted sample). b) Temperature dependence of the longitudinal resistivity.

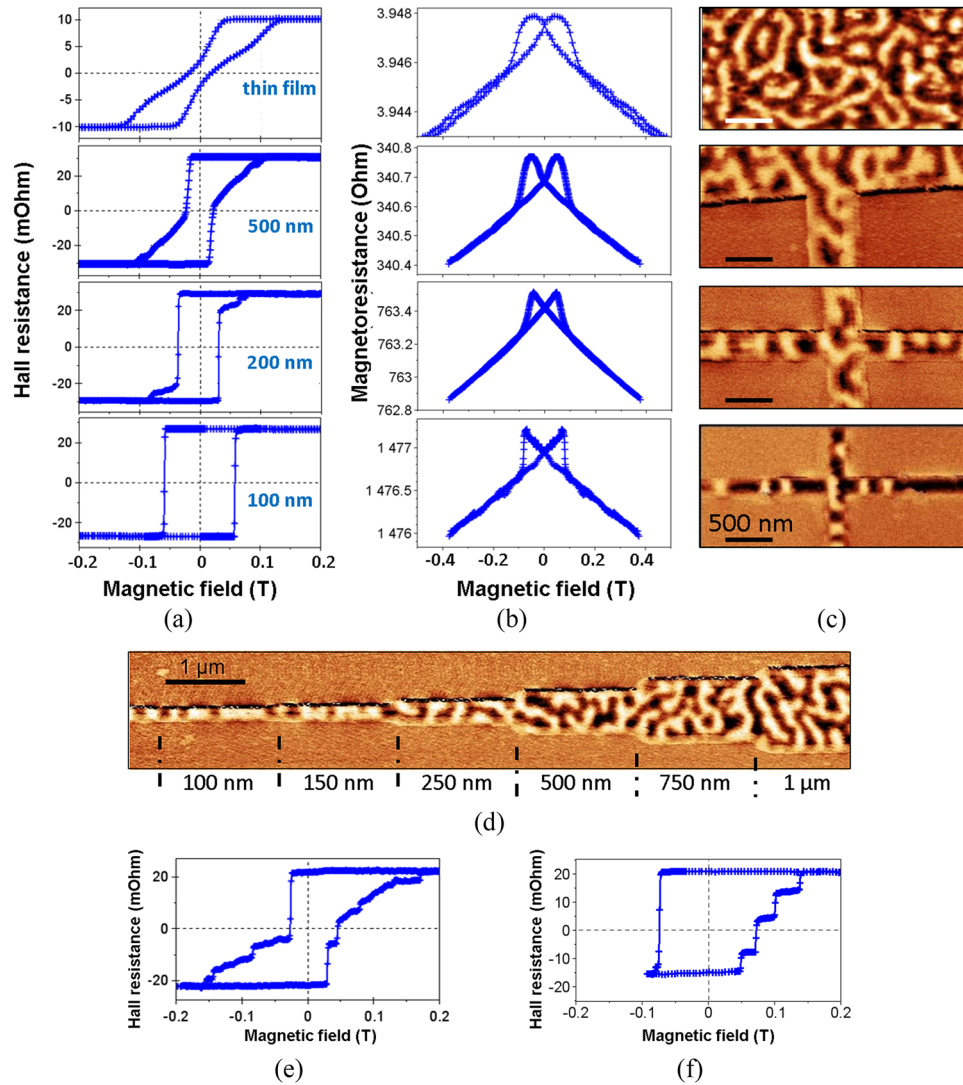


FIG. 3. a) EHE loops measured in the thin film and in crosses of various widths. b) Corresponding MR loops (measured with perpendicular magnetic field). c) MFM images of the corresponding structures in the as-grown magnetic state. d) MFM image of a structure consisting of wires of different widths, in the as-grown magnetic state. The nominal wire widths are indicated below the figure. e) EHE loop of a 200 nm wide cross at 10 K. f) EHE minor loop of a 100 nm wide cross at 10 K.

Several features appear when measuring the MR and EHE of patterned nanowires. Concerning the Hall measurements of Fig. 3a, the EHE angle is not modified, but there is strong dependence of the hysteresis loop with the wire width. The decrease of the wire width leads to an increase of the remanence, which is of 100 % for 500 nm-wide crosses, an increase of the coercive field, and a decrease of the saturation field. The reasons for this evolution will be discussed later.

As the MMR contribution is proportional to the product $\vec{M} \cdot \vec{B}$,³² these evolutions of the hysteresis loop are responsible for the evolutions of the MR loops of Fig. 3b, with in particular the sharpening of the MR loop for narrow widths.

Fig. 3c exhibits MFM observations performed on nanostructures of different widths. The imaging being made right after the nanoprocessing, the sample is still in the as-grown magnetic state. For the 200 nm-wide crosses, the DWs tend to align perpendicularly to the nanowire edges, in order to minimize the DW surface, and thus the anisotropy and exchange energy cost. At 100 nm, the magnetic state consists of magnetic domains separated by DWs orthogonal to the wire. This is the ideal configuration to realize current-induced DW propagation experiments. This effect can also be seen in the nanostructure of Fig. 3d, which consists in a single nanowire of varying width. The transition

occurs at a width comprised between 100 and 150 nm: when the wire width becomes smaller than the equilibrium domain width, the intertwined domain configuration is obviously unstable.

Let us now discuss the evolution of the loops observed in Fig. 3a for thin wires. A large decrease of the saturation field can be observed in thin wires, from 132 mT in thin films to 62 mT in 100 nm wide nanowires. This can be attributed to the decrease of demagnetizing field effects: while the demagnetizing field tends to prevent the magnetic saturation, in a very thin wire the effect is limited by the geometry.

Conversely, the coercivity increases in thin wires, from 15 mT to 56 mT. As discussed in Ref. 36, the main origin of this increase is the suppression of the available paths for DW propagation. The DW is moving in a disordered medium. In thin wires, the DW is forced to cross all the defects. In large wires, the DW somehow follows the easiest path during its propagation, since it can get around the biggest defects.

Note that at low temperature it becomes possible to observe Barkhausen jumps (cf. Fig. 3e and 3f), *i.e.*, the discrete motion of the DW from one pinning site to another.³⁶ The minor loop obtained in a 100 nm-wide cross shows 4 jumps. The EHE amplitudes of these jumps indicate that the DW reverses approximately a fifth of the cross for each jump, and thus that the typical distance between pinning sites is around 20 nm.

The increase of the coercivity in thin wires can also be seen in MFM images performed in remanent states, after magnetic saturation and partial reversal of the magnetization. Fig. 4a shows that the reversed magnetic domain, appearing in black and coming from a nucleation pad on the right side, does not propagate into the thinnest part of the wire. It can also be seen in Fig. 4b, where the injection and the propagation are more difficult in thinner nanowires.

Note that another effect can contribute to the enhancement of the coercivity: as nucleation centers are distributed randomly, the probability of a narrow area to contain a nucleation center is small. This effect tends to increase the nucleation field of smaller areas. For instance, in Fig. 4b there have been nucleation events in the large wires, but none in the two smaller wires.

In the 500 nm-wide nanowire of Fig. 4b, a single domain propagates in the wire. Interestingly, the DW does not switch the magnetization of the whole wire: as the width is larger than the equilibrium domain width, a multidomain magnetic configuration can be stabilized by the demagnetizing field.

This coercivity increase leads to the increase of the remanence seen in Fig. 3a, as it becomes difficult for a DW to reach the Hall cross. It is also responsible for the abruptness of the magnetization switching: at high fields, it becomes possible for the DW to reverse the magnetization of the whole cross.

To conclude, [Au (10 Å)/Co (6.6 Å)/Pd (10 Å)]₁₀ multilayers are promising candidates for current-induced DW experiments. Indeed, this new system exhibits a high perpendicular anisotropy,

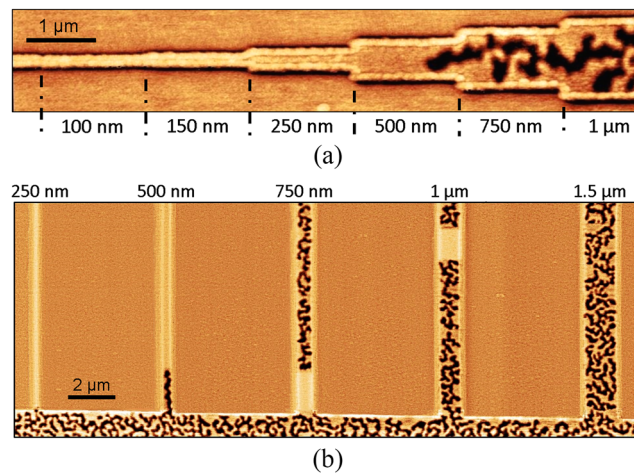


FIG. 4. a) MFM image of the structure consisting of wires of different widths, after saturation and partial magnetization reversal. b) MFM image of wires of different widths connected to a nucleation pad, after saturation and partial magnetization reversal.

a reasonable coercivity and a low resistivity. As the spin-orbit coupling of Pd is lower than that of Pt, one can expect lower damping constants in Pd-based systems, which could thus be an interesting alternative to Pt-based multilayers for current-induced DW propagation. The extraction of the DMI constant from DW energy estimation suggests that the DMI could be large enough to stabilize Néel walls or skyrmions. Furthermore, in sub-150 nm wires the magnetic configuration consists in series of parallel DWs, which is the ideal configuration to perform current induced DW motion experiments. Further experiments should allow quantifying more precisely the DMI strength, the spin transfer torque efficiency,¹ and the maximal DW velocity that can be obtained under current.

This work was partly supported by the French Agence Nationale de la Recherche (ANR) through Projects SPINHALL (2010-2013) and SOSPIN (2013-2016).

- ¹ A. Thiaville, S. Rohart, É. Jué, V. Cros, and A. Fert, *Europhys. Lett.* **100**, 57002 (2012).
- ² Y. Yoshimura, K. J. Kim, T. Taniguchi, T. Tono, K. Ueda, R. Hiramatsu, T. Moriyama, K. Yamada, Y. Nakatani, and T. Ono, *Nat. Phys.* **12**, 157–161 (2016).
- ³ S. Emori, U. Bauer, S. Ahn, E. Martinez, and G. Beach, *Nat. Mater.* **12**, 611 (2013).
- ⁴ T. H. Pham, J. Vogel, J. Sampaio, M. Vaňatka, J.-C. Rojas-Sánchez, M. Bonfim, D. S. Chaves, F. Choueikani, P. Ohresser, E. Otero, A. Thiaville, and S. Pizzini, *Europhys. Lett.* **113**, 67001 (2016).
- ⁵ S. Pizzini, J. Vogel, S. Rohart, L. D. Buda-Prejbeanu, E. Jué, O. Boulle, I. M. Miron, C. K. Safeer, S. Auffret, G. Gaudin, and A. Thiaville, *Phys. Rev. Lett.* **113**, 047203 (2014).
- ⁶ A. N. Bogdanov and U. K. Rößler, *Phys. Rev. Lett.* **87**, 037203 (2001).
- ⁷ S. Rohart and A. Thiaville, *Phys. Rev. B* **88**, 184422 (2013).
- ⁸ O. Boulle, J. Vogel, H. Yang, S. Pizzini, D. de Souza Chaves, A. Locatelli, T. Menteş, A. Sala, L. Buda-Prejbeanu, and O. Klein, *Nat. Nanotech.* **11**, 449–454 (2016).
- ⁹ A. Fert, V. Cros, and J. Sampaio, *Nat. Nanotech.* **8**, 152–156 (2013).
- ¹⁰ X. Zhang, M. Ezawa, and Y. Zhou, *Sci. Rep.* **5**, 9400 (2015).
- ¹¹ M. Heide, G. Bihlmayer, and S. Blügel, *Phys. Rev. B* **78**, 140403 (2008).
- ¹² S. Heinze, K. von Bergmann, M. Menzel, J. Brede, A. Kubetzka, R. Wiesendanger, G. Bihlmayer, and S. Blügel, *Nat. Phys.* **7**, 713–718 (2011).
- ¹³ N. Romming, C. Hanneken, M. Menzel, J. Bickel, B. Wolter, K. von Bergmann, A. Kubetzka, and R. Wiesendanger, *Science* **341**, 636–639 (2013).
- ¹⁴ N. Kiselev, A. Bogdanov, R. Schäfer, and U. Röyler, *J. Phys. D* **44**(39), 392001 (2011).
- ¹⁵ C. Moreau-Luchaire, C. Moutafis, N. Reyren, J. Sampaio, C. Vaz, N. Van Horne, K. Bouzehouane, K. Garcia, C. Deranlot, and P. Warnicke, *Nat. Nanotech.* **11**, 444 (2016).
- ¹⁶ S. Woo, K. Litzius, B. Krüger, M. Im, L. Caretta, K. Richter, M. Mann, A. Krone, R. Reeve, and M. Weigand, *Nat. Mater.* **15**, 501–506 (2016).
- ¹⁷ A. Neubauer, C. Pfleiderer, B. Binz, A. Rosch, R. Ritz, P. Niklowitz, and P. Böni, *Phys. Rev. Lett.* **102**, 186602 (2009).
- ¹⁸ G. Chen, T. Ma, A. N'Diaye, H. Kwon, C. Won, Y. Wu, and A. Schmid, *Nat. Commun.* **4**, 2671 (2013).
- ¹⁹ A. Hrabec, N. A. Porter, A. Wells, M. J. Benitez, G. Burnell, S. McVitie, D. McGrouther, T. A. Moore, and C. H. Marrows, *Phys. Rev. B* **90**, 020402 (2014).
- ²⁰ B. Dupé, G. Bihlmayer, M. Böttcher, S. Blügel, and S. Heinze, *Nat. Commun.* **7** (2016).
- ²¹ A. Soumyanarayanan, M. Raju, A. Oyarce, A. Tan, M. Im, A. Petrović, P. Ho, K. Khoo, M. Tran, and C. Gan, *Nat. Mater.* **16**(9), 898 (2017).
- ²² H. Yang, A. Thiaville, S. Rohart, A. Fert, and M. Chshiev, *Phys. Rev. Lett.* **115**, 267210 (2015).
- ²³ C. L. Canedy, X. W. Li, and G. Xiao, *Phys. Rev. B* **62**(1), 508 (2000).
- ²⁴ H. Tanigawa, T. Koyama, G. Yamada, D. Chiba, S. Kasai, S. Fukami, T. Suzuki, N. Ohshima, N. Ishiwata, Y. Nakatani, and T. Ono, *Appl. Phys. Express* **2**(5), 053002 (2009).
- ²⁵ B. Kaplan and G. A. Gehring, *J. Magn. Magn. Mater.* **128**, 111 (1993).
- ²⁶ V. Gehanno, Y. Samson, A. Marty, B. Gilles, and A. Chamberod, *J. Magn. Magn. Mater.* **172**, 26 (1997).
- ²⁷ M. Heide, G. Bihlmayer, and S. Blügel, *Phys. Rev. B* **78**(14), 140403 (2008).
- ²⁸ M. Belmeguenai, J. Adam, Y. Roussigné, S. Eimer, T. Devolder, J. Kim, S. Cherif, A. Stashkevich, and A. Thiaville, *Phys. Rev. B* **91**(18), 180405 (2015).
- ²⁹ M. Vaňatka, J.-C. Rojas-Sánchez, J. Vogel, M. Bonfim, M. Belmeguenai, Y. Roussigné, A. Stashkevich, A. Thiaville, and S. Pizzini, *J. Phys. Condens. Matter* **27**(32), 326002 (2015).
- ³⁰ J. P. Attané, M. Tissier, A. Marty, and L. Vila, *Phys. Rev. B* **82**(2), 024408 (2010).
- ³¹ J. Moritz, B. Rodmacq, S. Auffret, and B. Dieny, *J. Phys. D* **41**(13), 135001 (2008).
- ³² A. P. Mihai, J. P. Attané, A. Marty, P. Warin, and Y. Samson, *Phys. Rev. B* **77**, 060401 (2008).
- ³³ V. D. Nguyen, L. Vila, P. Laczkowski, A. Marty, T. Faivre, and J. P. Attané, *Appl. Phys. Lett.* **99**(26), 262504 (2011).
- ³⁴ V. D. Nguyen, L. Vila, P. Laczkowski, A. Marty, T. Faivre, and J. P. Attané, *Phys. Rev. Lett.* **107**, 136605 (2011).
- ³⁵ R. Danneau, P. Warin, J. P. Attané, I. Petej, C. Beigné, C. Fermon, O. Klein, A. Marty, F. Ott, Y. Samson, and M. Viret, *Phys. Rev. Lett.* **88**, 157201 (2002).
- ³⁶ J. P. Attané, D. Ravelosona, A. Marty, V. D. Nguyen, and L. Vila, *Phys. Rev. B* **84**(14), 144418 (2011).